

Characterization of laser-induced air plasmas by third harmonic generation

Cristina Rodríguez,* Zhanliang Sun, Zhenwei Wang, and Wolfgang Rudolph

Department of Physics and Astronomy, University of New Mexico, Albuquerque, NM 87131, USA

*crisrod@unm.edu

Abstract: Third harmonic generation by a weak femtosecond probe pulse intersecting a pump laser-induced plasma in air is investigated and a general model is developed to describe such signal, applicable to a wide range of focusing and plasma conditions. The effect of the surrounding air on the generated signal is discussed. The third-order nonlinear susceptibility of an air plasma with electron density N_e is determined to be $\chi_p^{(3)} = \chi_a^{(3)} + \gamma_p N_e$ with $\gamma_p = 2 \pm 1 \times 10^{-49} \text{ m}^5 \text{ V}^{-2}$ and $\chi_a^{(3)}$ being the third-order susceptibility in air. Lateral scans of the probe through the plasma are used to determine electron density profiles and the effect of focusing and phase mismatch is discussed.

© 2011 Optical Society of America

OCIS codes: (280.5395) Plasma diagnostics; (180.4315) Nonlinear microscopy; (320.2250) Femtosecond phenomena.

References and links

1. Y. Barad, H. Eisenberg, M. Horowitz, and Y. Silberberg, "Nonlinear scanning laser microscopy by third harmonic generation," *Appl. Phys. Lett.* **70**, 922–924 (1997).
2. A. N. Naumov, D. A. Sidorov-Biryukov, A. B. Fedotov, and A. M. Zheltikov, "Third-harmonic generation in focused beams as a method of 3D microscopy of a laser-produced plasma," *Opt. Spectrosc.*, **90**, 778–783 (2001).
3. S. Suntsov, D. Abdollahpour, D. G. Papazoglou, and S. Tzortzakis, "Filamentation-induced third-harmonic generation in air via plasma-enhanced third-order susceptibility," *Phys. Rev. A* **81**, 033817 (2010).
4. K. Hartinger and R. A. Bartels, "Enhancement of third harmonic generation by a laser-induced plasma," *Appl. Phys. Lett.* **93**, 151102 (2008).
5. S. Backus, J. Peatross, Z. Zeek, A. Rundquist, G. Taft, M. M. Murnane, and H. C. Kapteyn, "16-fs, 1-microJ ultraviolet pulses generated by third-harmonic conversion in air," *Opt. Lett.* **21**, 665–667 (1996).
6. R. W. Boyd, *Nonlinear Optics* (Academic Press, 2008).
7. J. F. Ward and G. H. C. New, "Optical third harmonic generation in gases by a focused laser beam," *Phys. Rev.* **185**, 57–72 (1969).
8. A. A. Fridman and L. A. Kennedy, *Plasma Physics and Engineering* (Taylor & Francis, 2004).
9. P. E. Ciddor, "Refractive index of air: new equations for the visible and near infrared," *Appl. Opt.* **35**, 1566–1573 (1996).
10. A. B. Fedotov, S. M. Gladkov, N. I. Koroteev, and A. M. Zheltikov, "Highly efficient frequency tripling of laser radiation in a low-temperature laser-produced gaseous plasma," *J. Opt. Soc. Am. B* **8**, 363–366 (1991).
11. J. Kasparian, R. Sauerbrey, and S. L. Chin, "The critical laser intensity of self-guided light filaments in air," *Appl. Phys. B* **71**, 877–879 (2000).
12. A. Talebpour, J. Yang, and S. L. Chin, "Semi-empirical model for the rate of tunnel ionization of N₂ and O₂ molecule in an intense Ti:sapphire laser pulse," *Opt. Commun.* **163**, 29–32 (1999).
13. S. Suntsov, D. Abdollahpour, D. G. Papazoglou, and S. Tzortzakis, "Efficient third-harmonic generation through tailored IR femtosecond laser pulse filamentation in air," *Opt. Express* **17**, 3190–3195 (2009).
14. Z. Sun, J. Chen, and W. Rudolph, "Determination of the transient electron temperature in a femtosecond-laser-induced air plasma," *Phys. Rev. E* **83**, 046408 (2011).
15. L. V. Keldysh, "Ionization in the field of a strong electromagnetic wave," *Sov. Phys. JETP* **20**, 1307–1314 (1965).

1. Introduction

Third harmonic generation (THG) microscopy [1] has been recognized as a useful nonlinear imaging modality to observe spatial inhomogeneities in both the linear (refractive index) and nonlinear (third-order susceptibility $\chi^{(3)}$) optical properties of materials, including biological species. Since all materials have a non-vanishing $\chi^{(3)}$, this technique can be applied to study virtually any material, as long as it is transparent at the wavelengths involved.

THG microscopy was applied to probe laser plasma plumes from solid targets [2], which are produced in laser induced breakdown spectroscopy for example. The potential of this technique from the standpoint of plasma diagnostics was suggested, but it remained unclear how the observed structures in the TH signal relate to plasma properties. There have been a number of experiments in which THG by a filament producing signal pulse was studied in the presence of a plasma string generated by an energetic pump in gaseous media (see for example [3,4]). This scenario is of potential interest for the generation of ultra-short pulses in the UV wavelength range (e.g. [5]). The two-order-of-magnitude increase of the THG efficiency in the presence of the pump induced plasma was attributed to a plasma-enhanced $\chi^{(3)}$ [3].

In this paper we investigate the third harmonic (TH) signal generated by a weak probe beam intersecting transversely a pump laser-induced plasma in air and develop a general model for the generation of such a signal, applicable for a wide range of focusing conditions and a radially symmetric distribution of the electron density (N_e). Unlike in previous experiments, the intensity of the probe pulse was chosen small enough such that filamentation was avoided and the TH signal was proportional to the probe intensity raised to the third power. This setup allowed us to study the properties of the pump-induced plasma and THG without interference by probe-induced filamentation and associated nonlinearities. We measure the functional dependence of the TH signal with respect to the electron density, estimate $\chi^{(3)}$ of such a medium, and propose a method by which the electron density distribution of a laser induced plasma can be measured with temporal resolution. The conditions under which THG can be used for 3D imaging of plasmas are evaluated and the limitations discussed.

2. Theoretical background

The TH field generated by a focused Gaussian fundamental beam propagating in an infinitely long homogeneous medium (material a) vanishes due to destructive interference of the TH waves generated before and after the focus, provided the material exhibits normal dispersion, see for example [6]

$$E_{3\omega}(z) = \frac{3i\omega E_\omega^3}{2n_{3\omega,a}c} \chi_a^{(3)} \int_{-\infty}^z \frac{\exp(i\Delta k_a z')}{(1 + iz'/z_{0,a})^2} dz' \quad \xrightarrow{z \rightarrow \infty} \quad 0, \quad (1)$$

where $\chi_a^{(3)}$ is the third-order nonlinear susceptibility of the medium, $n_{3\omega,a}$ is the refractive index at the TH frequency, E_ω is the fundamental Gaussian field amplitude, $\Delta k_a = 3k_{\omega,a} - k_{3\omega,a}$ is the wave-vector mismatch between the fundamental and TH waves, and $z_{0,a} = \pi n_{\omega,a} w_{0,a}^2 / \lambda$ is the Rayleigh length of the fundamental Gaussian beam, where $w_{0,a}$ corresponds to its beam waist.

A convenient way to visualize the value of the integral in Eq. (1) is using a vibrational diagram [7], as shown in Fig. 1(a), where the TH field $E_{3\omega}(z)$ is plotted in the complex plane, with z as the running parameter. For a particular z position the resultant TH field is represented by the vector from the origin to the corresponding point on the trace. As shown in Fig. 1(a) the TH field created in the negative half-space $-\infty < z < 0$ is canceled by the TH field created in the positive half-space $0 < z < +\infty$. As a result the integration over the infinite medium yields no THG.

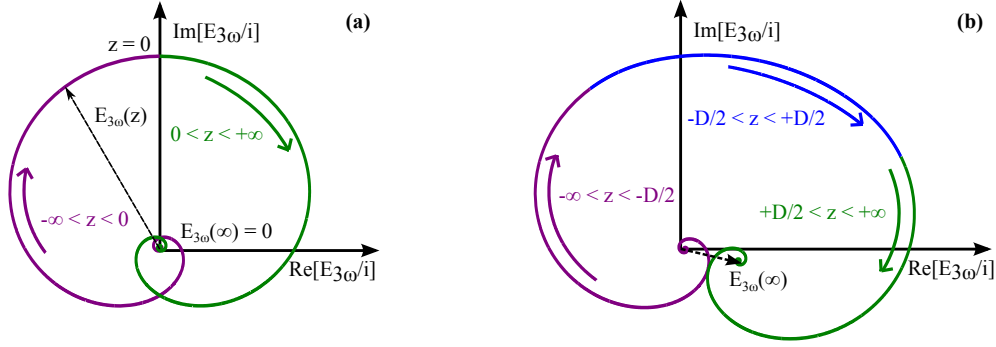


Fig. 1. Generated TH field as a function of position z . (a) For an infinite medium the integration over the entire space yields no net TH. (b) If a slab of a material of thickness D is introduced in the focus, the TH field no longer vanishes.

If a slab of a material of thickness D is introduced with different linear and/or nonlinear optical parameters, see Fig. 2, the TH field $E_{3\omega}$ will in general no longer vanish. The corresponding integral for the TH field can be split into three components - before the slab, the slab and after the slab. After adding the three contributions, taking into consideration that at the interface of two nonlinear media the phase mismatch between the fundamental and harmonic waves has to be continuous, the TH field takes on the form

$$\begin{aligned}
 E_{3\omega} = & \frac{3i\omega E_{\omega}^3}{2c} \left[t_{ap}^{3\omega} t_{pa}^{3\omega} \frac{\chi_a^{(3)}}{n_{3\omega,a}} \int_{-\infty}^{-\frac{D}{2}} \frac{\exp(i\Delta k_a Z)}{(1+iZ/z_{0,a})^2} dz \right. \\
 & + (t_{ap}^{\omega})^3 t_{pa}^{3\omega} \frac{\chi_p^{(3)}}{n_{3\omega,p}} \exp\left(i\frac{D}{2}[\Delta k_p - \Delta k_a]\right) \int_{-\frac{D}{2}}^{+\frac{D}{2}} \frac{\exp(i\Delta k_p Z)}{(1+iZ/z_{0,p})^2} dz \\
 & \left. + (t_{ap}^{\omega})^3 (t_{pa}^{\omega})^3 \frac{\chi_a^{(3)}}{n_{3\omega,a}} \exp(iD[\Delta k_p - \Delta k_a]) \int_{+\frac{D}{2}}^{+\infty} \frac{\exp(i\Delta k_a Z)}{(1+iZ/z_{0,a})^2} dz \right]. \quad (2)
 \end{aligned}$$

Here the subscripts p and a refer to the slab material and medium a , respectively. The coefficients $t^{\omega,3\omega}$ are the transmission factors for the fundamental and harmonic waves. We also allowed for an arbitrary position z_w of the beam waist by introducing $Z = z - z_w$. In Eq. (2) we assume a homogeneous distribution of both Δk_p and $\chi_p^{(3)}$ across the slab material. Figure 1(b) shows the corresponding vibrational diagram for this scenario. The total TH field at infinity does not vanish, contrary to the case shown in Fig. 1(a) for the infinitely long medium. Instead, the total TH field is a contribution from the TH generated in medium a and in the slab.

Using Eq. (2) we can calculate the TH field produced by a probe beam propagating through a plasma (material p) region in air (material a) centered around the focus of the probe. According to the Drude model the refractive index of the plasma at frequency ω can be written as [8]:

$$n_{\omega,p} = n_{\omega,a} - \frac{N_e}{2N_c}, \quad (3)$$

where $n_{\omega,a}$ is the refractive index of air at frequency ω , N_e is the electron density, and $N_c = \epsilon_0 m_e \omega^2 / e^2$ is the critical electron density where laser and plasma frequency are equal, e and m_e are the electron charge and mass, respectively. For $\lambda = 800$ nm, the critical electron density is $N_c \approx 1.8 \times 10^{27} \text{ m}^{-3}$.

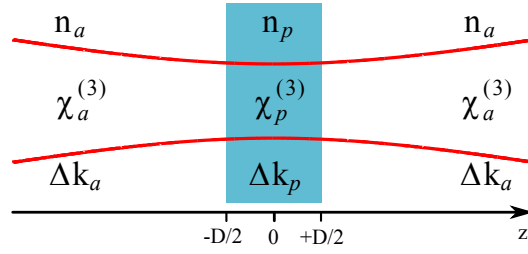


Fig. 2. Schematic diagram of a Gaussian beam propagating through a sample consisting of a host material in which a medium of thickness D is embedded.

From Eq. (3) the wave-vector mismatch in the plasma can be written as:

$$\Delta k_p = \Delta k_a + qN_e, \quad (4)$$

where $\Delta k_a = 3\omega(n_{\omega,a} - n_{3\omega,a})/c$ is the wave-vector mismatch in air and $q = -4\omega/(3cN_e)$.

The third-order nonlinear susceptibility of air can be estimated by $\chi_a^{(3)} \approx 5.7 \times 10^{-26} \text{ m}^2/\text{V}^2$ [7]. For the third-order nonlinear susceptibility of the plasma $\chi_p^{(3)}$ we make the following *ansatz*:

$$\chi_p^{(3)} = \chi_a^{(3)} + \gamma_p N_e, \quad (5)$$

where γ_p is a constant to be determined, representing the effective second order hyperpolarizability of a single electron in the plasma. This *ansatz* is consistent with the notion that the third-order susceptibility of the plasma $\chi_p^{(3)}$ is controlled by the scattering of quasi-free electrons by an effective nonlinear ionic potential in the presence of a laser field [10]. It assumes that the “background” nonlinearity of the neutral and ionic gas molecules is that of air. It is conceivable that for high electron densities terms of order N_e^2 and higher have to be added to account for electron-electron interactions, electron-ion interactions and a change in the background nonlinearity produced by the molecules.

Equation (2) holds for sufficiently weakly focused beams (numerical aperture $\text{NA} \lesssim 0.4$, corresponding to $w_0 \gtrsim 1 \mu\text{m}$), which is a consequence of $E_{3\omega}$ from Eq. (2) being the solution to the paraxial wave equation, and radially symmetric electron density distributions. Equation (2) can be simplified assuming $D \ll z_0$ to take on the form

$$E_{3\omega} = \frac{3i\omega E_\omega^3}{cn_{3\omega}} \exp\left(i\frac{D}{2}[\Delta k_p - \Delta k_a]\right) \left\{ \chi_a^{(3)} \left[i \sin\left(\frac{D}{2}[\Delta k_p - \Delta k_a]\right) \int_0^{+\infty} \frac{\exp(i\Delta k_a z)}{(1+iz/z_0)^2} dz \right. \right. \\ \left. \left. - \frac{D}{2} \cos\left(\frac{D}{2}[\Delta k_p - \Delta k_a]\right) \right] + \chi_p^{(3)} \frac{\sin[\frac{D}{2}\Delta k_p]}{\Delta k_p} \right\}, \quad (6)$$

where we made the approximations $n_{3\omega,p} \approx n_{3\omega,a} = n_{3\omega}$ in the prefactors, $z_{0,p} \approx z_{0,a} = z_0$, and assumed $t^{\omega,3\omega} \approx 1$ and $z_w = 0$. The first term in Eq. (6), with $\chi_a^{(3)}$ as a prefactor, represents the contribution from air, and the second term the contribution from the plasma. For low electron densities ($N_e \ll N_c$) as is typical for weakly ionized plasmas, and sufficiently small plasma thickness D , the phase mismatch $|\Delta k_p D| \ll 1$. This allows us to expand the trigonometric functions and the exponential prefactor in Eq. (6), using Eq. (4), to first order in N_e . We obtain

$$E_{3\omega} = \frac{3i\omega E_\omega^3}{2cn_{3\omega}} DN_e \left[iq\chi_a^{(3)} \int_0^{+\infty} \frac{\exp(i\Delta k_a z)}{(1+iz/z_0)^2} dz + \gamma_p \right]. \quad (7)$$

Since the TH signal $S_{3\omega} \propto |E_{3\omega}|^2$ we expect that $S_{3\omega} \propto N_e^2$ in the low electron density limit.

Figures 3(a) and 3(b) depict the calculated TH signal as a function of the electron density of a pump induced plasma ($D = 100 \mu\text{m}$) for weak and strong focusing conditions of the probe beam, respectively. The solid blue lines in Figures 3(a) and 3(b) show the exact results using Eq. (2), while the solid red lines neglect the contribution from air to the generated TH signal. For weak focusing conditions, Fig. 3(a), the contribution from air cannot be neglected. The TH generated in air and in the plasma are of the same order of magnitude but opposite signs. For tight focusing conditions, Fig. 3(b), the contribution from air is important for the low electron densities. Only for high electron densities this contribution becomes negligible, since the effect of the “quasi-free” electrons on the signal becomes dominant, cf. Eq. (5). In general, the air contribution can be approximately neglected if $(\gamma_p N_e D)/(2\chi_a^{(3)} z_0) \gg 1$, where the factors $(\gamma_p N_e D)$ and $(2\chi_a^{(3)} z_0)$ are an approximate measure of the magnitude of the signal generated in the plasma and air, respectively.

The dotted line in Fig. 3(a) shows a parabolic fit, confirming that $S_{3\omega} \propto N_e^2$ in the low electron density limit. For electron densities $N_e > 10^{24} \text{ m}^{-3}$ and $D = 100 \mu\text{m}$, $|\Delta k_p D| \gtrsim 1$ and the approximations leading to Eq. (7) are not valid. The oscillations of the TH signal are a consequence of the phase mismatch approaching and exceeding π .

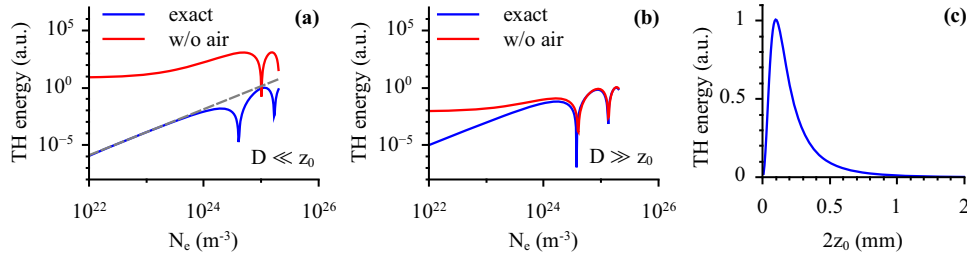


Fig. 3. TH signal as a function of N_e for (a) weak focusing conditions, $D \ll z_0$, and (b) tight focusing conditions, $D \gg z_0$, using Eq. (2), solid blue line, and Eq. (2) neglecting the contribution from air, solid red line. The dashed line in (a) shows a parabolic fit. (c) TH signal as a function of $2z_0$ for $N_e = 1.5 \times 10^{23} \text{ m}^{-3}$ and $D = 100 \mu\text{m}$.

Figure 3(c) shows the TH signal as a function of the confocal parameter $2z_0$ for constant probe energy. If focused tightly, the probe will generate TH in a small volume, representing a small fraction of the plasma, with the limiting case where the TH signal becomes negligible for a bulk sample. For large z_0 the small probe intensity prevents efficient THG. Optimal focusing conditions are found for $2z_0 \approx D$, for the case where $|\Delta k_p D| \ll 1$.

In typical experimental conditions the electron density distribution is not constant along z , $N_e(z) = N_e f(z)$. Such an electron density distribution produces a gradient in the plasma non-linearity $\chi_p^{(3)}(z)$, cf. Eq. (5), and in the wave-vector mismatch $\Delta k_p(z)$, cf. Eq. (4). The total TH field can be calculated using a relation similar to Eq. (2). The integral corresponding to the plasma region is split into smaller regions of thickness Δz within which $N_e(z)$ can be regarded constant. As before, when adding these contributions, the accumulated phase in one region has

to be correctly added to the phase in the following region. The TH field takes on the form

$$E_{3\omega} = \frac{3i\omega E_{\omega}^3}{2cn_{3\omega}} \left\{ \chi_a^{(3)} \int_{-\infty}^{-\frac{D}{2}} \frac{\exp(i\Delta k_a z)}{(1+iz/z_0)^2} dz + \exp\left[-i\frac{D}{2}\Delta k_a\right] \Delta z \sum_{m=1}^M \frac{\exp[i\Delta k_p(z_m)\Delta z]}{(1+iz_m/z_0)^2} \chi_p^{(3)}(z_m) + \chi_a^{(3)} \exp[-iD\Delta k_a] \exp\left[i \sum_{m=1}^M \Delta k_p(z_m)\Delta z\right] \int_{+\frac{D}{2}}^{+\infty} \frac{\exp(i\Delta k_a z)}{(1+iz/z_0)^2} dz \right\}, \quad (8)$$

where $z_m = -\frac{D}{2} + (m-1)\Delta z$ and $\Delta z = D/(M-1)$, with $m = 1, 2, \dots, M$. Under these conditions it is still possible to show analytically that $S_{3\omega} \propto N_e^2$, in the low electron density limit, by expanding the exponential factors containing Δk_p in Eq. (8) to first order in N_e .

3. Experimental setup

The experiments were carried out using a Ti:sapphire chirped-pulse-amplification laser system providing 40-fs, 800-nm pulses, with energies of 2 mJ, at a 1-kHz repetition rate. The pulse to pulse energy variations of the laser were $\sim 2\%$. A schematic diagram of the experimental setup is shown in Fig. 4. The output from the amplifier was split into a pump and a probe pulse. The

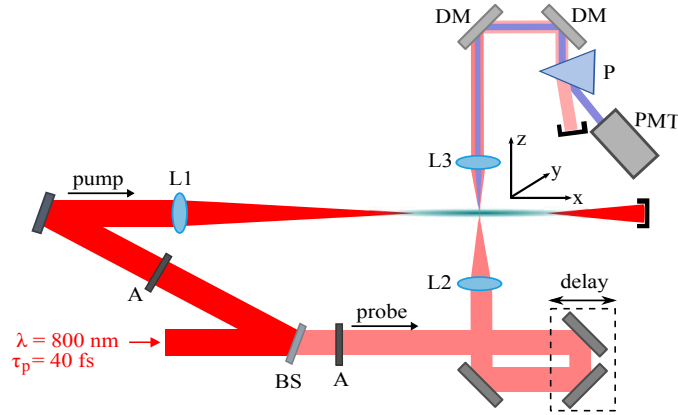


Fig. 4. Schematic diagram of the experimental setup to measure THG by a probe pulse intersecting transversely a pump pulse produced plasma. L1, L2, L3, lenses; BS, beam splitter; DM, dichroic mirror; A, variable attenuator; P, prism; PMT, photomultiplier tube.

pump pulse with an energy of up to 1.5 mJ was focused using a lens L1, generating a plasma in air. The beam waist of the probe pulse after passing through lens L2 intersected the plasma transversely. The beam waist of the probe was determined through knife-edge measurements. The time delay between the pump and probe pulses was adjusted using an optical delay line. The TH signal was filtered from the fundamental using dichroic mirrors, a prism, and an interference filter, and was detected by a photomultiplier tube (PMT). The background (measured when blocking the pump beam) was subtracted from the measured TH signal. For a time delay of 30 ps the signal-to-background ratio was $\sim 100 : 1$.

4. Results and discussion

Figure 5 shows the TH signal as a function of the probe pulse energy with a pump induced plasma present. This 10-cm long plasma of diameter $D \approx 140 \mu\text{m}$ was produced by 1.5 mJ pulses using a lens L1 with $f = 1$ m. The probe was focused with an $f = 30$ -cm lens (L2)

producing a beam waist of $w_0 \approx 17 \mu\text{m}$ at $z_w = 0$. For small probe energies ($\lesssim 5 \mu\text{J}$) the TH signal shows the expected cubic dependence. For larger energies the slope is less than three, which was also observed in [13] and is likely a consequence of the generation of a plasma by the probe and subsequent probe defocusing. From experimentally obtained ionization rates of N_2 and O_2 as a function of laser intensity [11,12], we can estimate $N_e \approx 4 \times 10^{24} \text{m}^{-3}$ at probe energies of about $20 \mu\text{J}$.

In the experiments to be described below where we used THG as a diagnostic tool the probe intensity was kept sufficiently small. This ensured that the TH signal generated by the probe alone was negligible compared to the case where a pump induced plasma was present and that the cubic power relationship applied. For example, for a probe energy of $1.7 \mu\text{J}$ under the focusing conditions of Fig. 5 and no plasma present, the TH signal was below our detection limit. From experimentally obtained ionization rates of N_2 and O_2 as a function of laser intensity [11,12], we estimate $N_e \approx 3 \times 10^{17} \text{m}^{-3}$ for such a probe pulse.

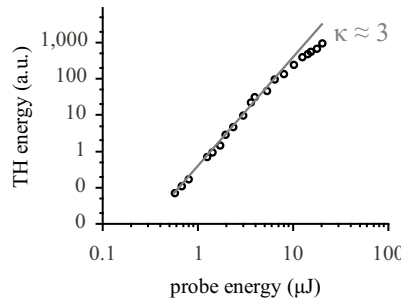


Fig. 5. TH signal as a function of the probe energy with a pump induced plasma present. The solid line shows a power law with $\kappa \approx 3$ as expected for THG.

In order to investigate the relationship of TH conversion and the electron density of the plasma, we measured the TH signal as a function of the time delay τ between pump and probe pulses and determined the time-dependent electron density in the plasma $N_e(\tau)$ by means of a diffraction experiment [14]. This experiment used the fact that the plasma induced diffraction of the zero-spatial frequency component of a probe beam is proportional to $N_e(\tau)$. We used an $f = 30\text{-cm}$ focusing lens (L2) for the probe producing a beam waist of $\approx 17 \mu\text{m}$ at $z_w = 0$. The laser amplifier repetition rate was reduced to 250 Hz to avoid thermal effects (see below). Figure 6 shows the so obtained TH signal from the probe as a function of the electron density in the plasma. The solid line illustrates the good agreement between the experiment and the predictions from Eq. (8). The simulations also took into account the change of the electron density spatial profile [14]. $N_e(z)$ changes from Gaussian at large $N_e(0)$ (small delays) to a more flat-top profile for low $N_e(0)$ (large delays) because of the bimolecular nature of the electron-ion recombination.

To estimate the plasma nonlinearity $\chi_p^{(3)}$ we compared the measured TH conversion efficiency as a function of electron density (Fig. 6) with the model predictions, according to Eq. (8). From Eq. (5) we obtained $\gamma_p = 2 \pm 1 \times 10^{-49} \text{m}^5 \text{V}^{-2}$, where the main sources of error came from the uncertainties on the beam waist and M^2 value of the probe, and on $\chi_a^{(3)}$. For electron densities of fs pulse induced filaments in air ($N_e \approx 1.5 \times 10^{23} \text{m}^{-3}$ [14]) the third-order nonlinear susceptibility is estimated to be $\chi_p^{(3)} \approx 8.7 \times 10^{-26} \text{m}^2/\text{V}^2$, a value that is approximately 1.5 times greater than the third-order nonlinear susceptibility of air, $\chi_a^{(3)} \approx 5.7 \times 10^{-26} \text{m}^2/\text{V}^2$ [7]. This result means that the effective second order hyperpolarizability of a single

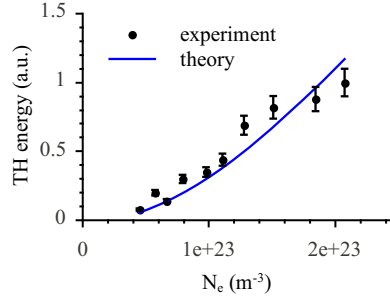


Fig. 6. TH signal as a function of the electron density in the plasma. The solid line shows simulation results based on Eq. (8). Because the profiles changed with delay, the TH signal does not scale quadratically with the electron density.

“quasi-free” electron in the plasma is about 70 times larger than that of an average air molecule ($\gamma_p \approx 70 \times \chi_a^{(3)} / N_{\text{air}}$ where N_{air} is the total number of air molecules $\approx 2 \times 10^{25} \text{ m}^{-3}$). In reference [3] an estimate for $\chi_p^{(3)}$ of $4.5 \pm 3 \times 10^{-24} \text{ m}^2/\text{V}^2$ was reported for $N_e \approx 2 \times 10^{25} \text{ m}^{-3}$, in agreement with what we obtain using our value for γ_p and Eq. (5).

In order to determine the spatial distribution of the electron density in a laser produced plasma, the TH signal was recorded while the plasma was scanned laterally (y direction) across the probe beam, which was realized by moving the focusing lens of the pump beam (L1) along the y direction using a translation stage. This resulted in the filament moving by the same amount Δy with respect to the probe beam, which is only true in the vicinity of the focal plane of lens L1, in which case aberrations and a change in the time delay between pump and probe beams can be neglected. The results of the scan are shown in Fig. 7. We used an $f = 30\text{-cm}$ focusing lens (L2) for the probe producing a beam waist of $\approx 17 \mu\text{m}$ at $z_w = 0$. The solid line in

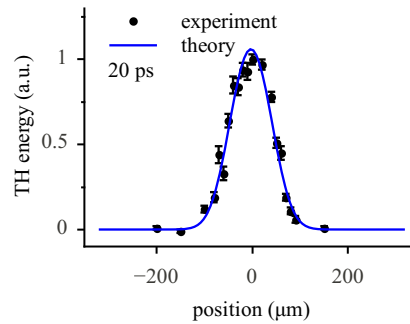


Fig. 7. TH signal obtained by scanning the probe laterally (y direction) through the plasma ($\tau = 20 \text{ ps}$). The solid line shows simulation results based on Eq. (8).

Fig. 7 was obtained from Eq. (8), and shows a distribution with a width of $\approx 100 \mu\text{m}$. For each y position we assumed a constant N_e over the probe beam with respect to y and integrated over z . Since $S_{3\omega}(y) \propto N_e^2(y)$ the spatial distribution shown in Fig. 7 corresponds to $N_e^2(y)$. From this we obtain that the spatial distribution of $N_e(y)$ has a width of $\approx 140 \mu\text{m}$.

It should be mentioned that for repetition rates $\gtrsim 500 \text{ Hz}$ the TH scan profiles exhibit pedestals extending over about 1 mm. We attribute this to an increase in the temperature of the air surrounding the plasma. Our THG model, Eq. (8), predicts a TH contribution from an

air channel with a refractive index and nonlinear susceptibility gradient expected from a temperature and resulting particle density gradient. To avoid this, the laser amplifier repetition rate was set to 250 Hz (Figures 6 and 7).

To study THG for higher plasma densities we generated an air plasma of a few mm length by focusing the pump pulse with a 10-cm-focal-length lens L1, cf. Fig. 4. The probe beam was focused using a 6-cm-focal-length lens (L2) producing a waist of $\approx 6 \mu\text{m}$. The laser amplifier repetition rate was set to 1 kHz, since the thermal effects were negligible under these experimental conditions. Figure 8 shows the TH signal while the plasma was scanned laterally (y direction) across the probe beam for several pump pulse energies (left column), and simulation results (right column).

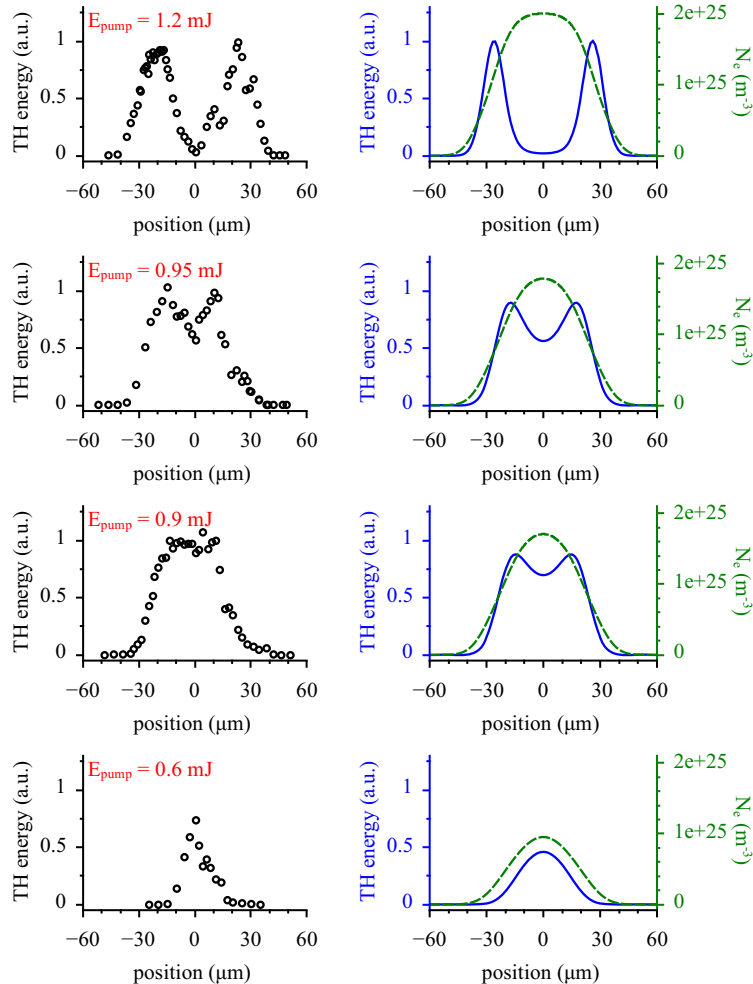


Fig. 8. TH signal obtained by scanning the probe laterally through the plasma for different pump energies (left column) and a pump-probe delay of 1.5 ps. The solid line (right column) shows simulation results based on Eq. (8). The dashed line shows the spatial electron density distribution obtained from a multi-photon ionization model in air.

To simulate the TH signal as a function of the scan coordinate we first estimated the electron

density distribution from Keldysh theory [15] assuming a Gaussian pump intensity of waist $w_0 \approx 50 \mu\text{m}$, a value larger than the predicted waist generated by a 10-cm-focal-length lens. For the high intensities used, however, the generation of a plasma and subsequent defocusing prevents the pump from reaching such small waists. The value assumed for the simulations was chosen based on the best agreement found between the simulations and the experimental results. It should be noted that the pump intensities involved lead to tunneling ionization and are higher than intensities for which rates have been determined experimentally [12]. The simulated electron densities are shown in the right column (dashed lines). These electron density distributions $N_e f(y, z)$ were then used in Eq. (8) to obtain the TH signal, which is shown as a solid line. We find good overall qualitative agreement between the model predictions and the experimental data. For the higher pump energies $N_e(y, z)$ broadens and its peak value increases. The model predicts local minima of the TH produced in the plasma center even though this is where $N_e(y, z)$ peaks, which is a consequence of the phase mismatch exceeding π , cf. Fig. 3(a). Therefore, structure found in the TH signal of high-density plasmas does not necessarily point to similar structures in the electron density itself.

In the low density regime, cf. Fig. 7, and assuming cylindrical symmetry of the plasma, the lateral scans can be used to measure plasma density distributions with temporal resolution by measuring $\chi_p^{(3)}$ and using Eq. (5) as a function of pump-probe delay. This approach is advantageous over fluorescence techniques, for example, where the response time is given by the shorter of the integration time of the detector and the fluorescence lifetime.

The question arises whether microscopic 3D imaging of plasmas using THG is possible. To resolve feature sizes Δz one would need focusing conditions of the probe for which the confocal parameter $2z_0 \lesssim \Delta z$. At the same time, to ensure $S_{3\omega} \propto N_e^2$ for unambiguous interpretation, $\Delta k_p \Delta z \ll 1$ is required. On the other hand, if $2z_0 \ll \Delta z$ the TH field would vanish due to destructive interference of the TH waves generated before and after the focus, adding another source of ambiguity in interpreting the structure found on the TH signal. As an example, boundaries of relatively uniform regions of thickness $D \gg 2z_0$ and individual structures with dimensions $\ll 2z_0$ separated by D could give rise to similar TH signals. In certain cases this ambiguity could be addressed by performing series of scans with different focusing conditions and scan directions. The detection limit of the experiment will dictate how strong the probe beam can be focused while keeping the intensity small enough to ensure a cubic power law for the TH conversion and to avoid significant contributions to the TH signal in the absence of the pump. As an example, for an air plasma with an electron density $N_e = 10^{25} \text{ m}^{-3}$, the upper limit on the dimension D which can be probed without ambiguities using a single lateral scan is $D \approx 1/\Delta k_p \approx 16 \mu\text{m}$.

In conclusion, 3D mapping of plasma densities using THG can be done for certain plasma symmetries, such as those found in air-filaments, where single scans can provide this information, along with modeling when necessary.

It is worth mentioning that the methods and results described in this work are not restricted to femtosecond laser-induced plasmas. This methodology can be applied, for example, to study plasmas generated from a nanosecond pulsed laser using a femtosecond probe, so long as both sources are synchronized.

5. Summary

A model of THG by a probe in the presence of a pump induced plasma was developed that can be applied to a wide range of focusing and plasma conditions. Contributions to the TH signal from the plasma and ambient gas can be distinguished and their relative strength depends on probe beam parameters and plasma size and density. When the probe is weakly focused the contribution from ambient gas molecules cannot be neglected. For higher density plasmas

and when the probe is tightly focused the contribution from ambient gas molecules becomes negligible. In general, we conclude that the air contribution can be approximately neglected if $(\gamma_p N_e D) / (2\chi_a^{(3)} z_0) \gg 1$. To use THG as plasma probe, care must be taken to keep the probe pulse fluence small enough to ensure a cubic power law for the TH conversion and to avoid significant contributions to the TH signal by the focused probe in the absence of the pump. Using this probe regime, $\chi_p^{(3)} = \chi_a^{(3)} + \gamma_p N_e(z)$ with $\gamma_p = 2 \pm 1 \times 10^{-49} \text{ m}^5 \text{ V}^{-2}$ was determined for the third-order susceptibility of the plasma. Under certain conditions (cylindrically symmetric plasma, phase mismatch $\ll 1$, and a confocal parameter of the probe approximately equal to the size of the plasma), lateral scans of the probe beam through the plasma can be used to determine 2D plasma density profiles with sub picosecond time resolution. In the general case, phase mismatch critically affects the scan profiles and must be taken into account to derive electron density profiles. 3D mapping of plasma densities using THG seems possible when additional information is available, such as the peak densities and approximate dimension of the structures. The latter could be obtained via modeling or confocal fluorescence imaging combined with up-conversion if temporal resolution is needed.

Acknowledgments

We are grateful to L. Emmert, D. Cremers, and R. Multari for helpful discussions and we thank J. Chen for support with the experiments. This work was supported by NSF (PHY-0722622) and ONR (N000140810350).